Superconductivity coupling of harmonic resonant oscillators: Homogeneous and heterogeneous extreme multistability with multi-scrolls ⊘

T. Fonzin Fozin 🗷 💿 ; A. R. Tchamda 💿 ; G. Sivaganesh 💿 ; K. Srinivasan 💿 ; Z. Tabekoueng Njitacke 🗓 ; A. B. Mezatio



Check for updates

Chaos 34, 013148 (2024)

https://doi.org/10.1063/5.0176928









Superconductivity coupling of harmonic resonant oscillators: Homogeneous and heterogeneous extreme multistability with multi-scrolls

Cite as: Chaos **34**, 013148 (2024); doi: 10.1063/5.0176928 Submitted: 18 September 2023 · Accepted: 27 December 2023 · Published Online: 29 January 2024







T. Fonzin Fozin,^{1,a)} A. R. Tchamda,² G. Sivaganesh,³ K. Srinivasan,⁴ Z. Tabekoueng Njitacke,⁵ and A. B. Mezatio⁶

AFFILIATIONS

- ¹ Department of Electrical and Electronic Engineering, Faculty of Engineering and Technology (FET), University of Buea, P.O. Box 63, Buea, Cameroon
- ²Department of Rural Engineering, Faculty of Agronomy and Agricultural Sciences, University of Dschang, P.O. Box 222, Dschang, Cameroon
- ³Department of Physics, Alagappa Chettiar Government College of Engineering and Technology, Karaikudi 630003, Tamilnadu, India
- ⁴Department of Physics, Nehru Memorial College (Affiliated to Bharathidasan University, Tiruchirapalli 620024, Tamilnadu, India), Puthanampatti, Tiruchirapalli 621007, Tamilnadu, India
- ⁵Department of Electrical and Electronic Engineering, College of Technology (COT), University of Buea, P.O. Box 63, Buea, Cameroon
- ⁶South-Polytech (Affiliated to École National Supérieur Polytechnique de Douala, Université de Douala, Douala, Cameroun), Institut Universitaire des Grandes Écoles des Tropiques, P.O. Box 25080, Douala, Cameroun

ABSTRACT

Understanding and characterizing multistabilities, whether homogeneous or heterogeneous, is crucial in various fields as it helps to unveil complex system behaviors and provides insights into the resilience and adaptability of these systems when faced with perturbations or changes. Homogeneous and heterogeneous multistabilities refer, respectively, to situation in which various multiple stable states within a system are qualitatively similar or distinct. Generating such complex phenomena with multi-scrolls from inherent circuits is less reported. This paper aims to investigate extreme multistability dynamics with homogeneous and heterogeneous multi-scrolls in two coupled resonant oscillators through a shunted Josephson junction. Analysis of equilibrium points revealed that the system supports both hidden and self-excited attractors. Various dynamical tools, including bifurcation diagrams, spectrum of Lyapunov exponents, and phase portraits, are exploited to establish the connection between the system parameters and various complicated dynamical features of the system. By tuning both system parameters and initial conditions, some striking phenomena, such as homogeneous and heterogeneous extreme multistability, along with the emergence of multi-scrolls, are illustrated. Furthermore, it is observed that one can readily control the number of scrolls purely by varying the initial conditions of the investigated system. A multi-metastable phenomenon is also captured in the system and confirmed using the finite-time Lyapunov exponents. Finally, the microcontroller implementation of the system demonstrates strong alignment with the numerical investigations.

Published under an exclusive license by AIP Publishing. https://doi.org/10.1063/5.0176928

Systems capable of generating hybrid multistability features are more attractive. In addition, if the system is electronically simple and possesses high dynamic complexity, it is, therefore, valuable for engineering applications. In this work, homogeneous and heterogeneous extreme multistabilities with multi-scrolls are reported. The tri-transient phenomenon is also captured, thereby enriching the existing literature. Such striking features are uncovered in two coupled resonant oscillators through a shunted

a) Author to whom correspondence should be addressed: fozintheo@gmail.com

Josephson junction. The results of the model have been demonstrated through laboratory measurements and do not solely rely on theoretical investigations or simulations.

I. INTRODUCTION

The design of innovative chaotic systems and circuits has received a great deal of attention in recent decades. ¹⁻⁴ Based on what has been published so far, such innovative systems are either designed to exhibit novel traits or to be straightforward.⁵ In this regard, in addition to artificial systems created entirely from scratch, numerous others are obtained by modifying or altering certain system parameters, such as their nonlinearity.⁶⁻⁸ Memristors⁹⁻¹² and the Josephson junction (JJ)^{13,14} are two prominent nonlinearities discussed in the literature to date that are becoming more and more significant in producing complicated dynamics.

The Josephson junction was first predicted in 1962¹⁵ and is constituted of superconducting materials that behave nonlinearly as a result of copper-pair quantum tunneling via a tiny insulating barrier. A few of its appealing characteristics comprise a high operational frequency, extremely minimal noise, and minimal power usage. Extensive research efforts have been devoted to the JJ devices in order to determine how they might be used in metrology, computing, and electronics. Additionally, the JJ has been found to play a crucial role in the development of essential technological components, such as quantum-computing devices, highly sensitive detectors, electronic components with superconductivity, and signal generators capable of producing high-speed chaotic signals, to name a few. 19-21

Apart from being investigated solely through their various existing models²² and references therein, circuits based on JJ devices are also at the forefront of several research projects. One can cite the relevant work of Louodop and collaborators,²³ where the authors discuss a JJ as a nonlinear component in a straightforward non-autonomous CLC resonator. Their results include the interesting phenomenon of extreme multistability, classified later as heterogeneous. Following the same approach, Refs. 24 and 25 have also considered the JJ as a nonlinear element in their proposed systems. The resistive capacitive shunted and linear resistive-capacitive-inductance shunted junctions were considered in each of those works. Additionally, both works share the special feature of having a simple electronic circuit with rich dynamical behaviors; for instance, in Ref. 24, one can note the coexistence of multi-scrolls and the homogeneous multistability in their system among the significant outcomes emphasized. Meanwhile, in Ref. 25, authors were able to tackle the striking phenomenon of hyperchaos in their system both with numerical simulations and microcontroller implementation. Regarding the aforementioned works, it is possible to make the following observations: The proposed or explored systems are either non-autonomous or are limited to demonstrate homogeneous or heterogeneous multistability. Also, most of those systems display muti-scrolls among their features.

Various relevant works in the literature have focused on the broadband application of double scrolls and multi-scrolls in several nonlinear dynamical systems, including random bit generations²⁶ and network optimization.²⁷ Chaotic multi-scrolls show more

interest since the phase trajectory of the dynamic can randomly jump between different scrolls, making it very unpredictable with the possibility of generating a much larger secret key space.²⁸ Multiscrolls are most often obtained through systematic modification of the nonlinearity function of the investigated systems or circuits.^{27,29} The enigmatic Chua's circuit has been extensively exploited both theoretically and experimentally as a study case in demonstrating the feasibility and generation mechanisms of n-scrolls.^{30,31} According to the general theory, multi-scroll chaotic attractors can be created by altering the nonlinear characteristics of a scroll-based chaotic attractor, resulting in multiple equilibrium points. Among existing methods, one can cite that of inserting various breakpoints in the system's nonlinear function to construct multi-scroll attractors..^{30,31} Also, the association of step³² and tangent hyperbolic functions^{33,34} was exploited to successfully generate grids of multi-scrolls in some investigated systems. In a more recent work, the authors of Ref. 28 have proposed a new technique based on a series of multi-level-logic pulse functions for generating symmetric multi-scrolls in a magnetized Hopfield neural network. Other methods of generating multi-scrolls are to consider nonlinearities in the form of hysteresis, saturated function series,³⁵ or sine function.³⁶ So far, nonlinearity seems to be the cornerstone in generating multiscroll in nonlinear systems. Nevertheless, the primary obstacle in designing multi-scrolls lies in the synthesis of nonlinearity using an electrical component. This prompts the inquiry of whether there exists an electrical apparatus capable of facilitating the creation of a multi-scroll chaotic attractor. The answer came with the JJ^{36,37} that possesses such nonlinearity. Since then, several works have reported multi-scroll exploiting the JJ as a nonlinear element. It was also found that multistability is inherent to those systems.

Multistability is one of the most popular venues in chaos theory. This happens when various initial conditions yield qualitatively distinct steady states for the same set of parameters. Symmetric systems are particularly prone to multistability, as any nonsymmetric attractor will always have a corresponding twin.³⁸ More attention is now dedicated to the analysis of multistability in systems given the disastrous consequences it might lead in practical applications. 11,39 This also represents the unpredictability of the system's behavior, adding to its complexity. Multiple attractors are a manifestation of parallel branches and hysteresis dynamics. 40,41 From recent trends, multistable systems are classified as heterogeneous or homogeneous. 42-44 The latter is a situation where coexisting attractors are of the same shape, while the former is the coexistence of different shapes or states. The coexistence of homogeneous and heterogeneous multistability suggests a rich and diverse landscape of stability and dynamics in natural and artificial systems. It showcases the intricate interplay of stability and resilience, shedding light on the system's ability to navigate various configurations while adapting to changing conditions. According to the author's knowledge, very few studies have reported systems or circuits capable of generating multi-scrolls with both homogeneous and heterogeneous multistabilities.⁴⁵ More importantly, most of these reported systems are designed artificially with no backbone on a real circuit. 36,3

In this work, a new system made of two coupled harmonic oscillators through a shunted JJ is designed. The sinusoidal non-linearity of the system provides flexibility in generating extreme multistability with self-excited and hidden dynamics. One of the

striking features highlighted is that the system exhibits both homogeneous and heterogeneous multistabilities while varying system parameters and/or initial conditions. Metastability with tri-transient chaos was also captured during our investigations. Implemented hardware further validated these prominent findings.

The remaining sections of this work are organized as follows. Section II focuses on the circuit description and mathematical modeling of the proposed system. Some basic properties, including phase space volume, analysis of equilibrium points, and system symmetry, are also analyzed. In Sec. III, numerical investigations are reported. The striking phenomena of heterogeneous and homogeneous multistabilities with multi-scrolls are discussed in Secs. IV and V, respectively. In Sec. VI, we report the rare phenomenon of tri-transient chaos. Section VII is dedicated to the hardware experiment. Finally, significant conclusions are presented in Sec. VIII.

II. CIRCUIT ANALYSIS AND ITS MATHEMATICAL MODEL

A. Circuit analysis

The circuit diagram in Fig. 1 consists of two coupled resonant harmonic oscillators (L_1C_1 and L_2C_2) through an ideal shunted Josephson junction (JJ) element.^{36,46} The JJ component is highly attractive nowadays given its capability to produce chaotic dynamics^{47,48} and attractors with multiple scrolls. In the schematic diagram of Fig. 1, the JJ is considered the only nonlinear component in the circuit and is marked by "X." The two harmonic oscillators are considered stable (i.e., no dissipative component). One of the main control parameters throughout this work will be the shunted resistance of the JJ element (i.e., the negative impedance converter $Z = -R^{49}$). Upcoming investigations will reveal that the JJ element is responsible for the emergence of the complex dynamical behaviors, including extreme multistability and multi-scrolls in system (4) (see Sec. III).

B. Mathematical model

The current in the JJ is described by

$$I = I_c \sin(\phi), \tag{1}$$

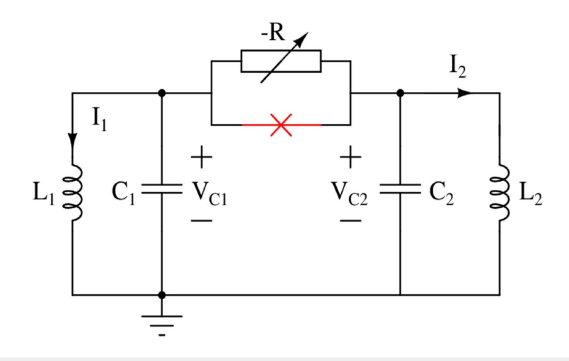


FIG. 1. Schematic diagram depicting the coupled resonant oscillators L_1C_1 and L_2C_2 through a shunted Josephson junction.

where

$$\frac{d\phi}{dt} = \frac{2e}{\hbar}V. (2)$$

Here, ϕ and V represent the phase angle and the potential drop across the JJ, respectively, while \hbar ($\hbar=h/2\pi$) and e represent the reduced Planck's constant and the charge of the electron. The dynamics of the proposed circuit can be described by a set of coupled differential equations [see Eq. (3)] when Kirchhoff's laws are applied to the circuit diagram shown in Fig. 1,

$$\begin{cases} L_{1} \frac{dI_{1}}{dt} = V_{C_{1}}, \\ L_{2} \frac{dI_{2}}{dt} = V_{C_{2}}, \\ C_{1} \frac{dV_{C_{1}}}{dt} = \frac{V_{C_{1}} - V_{C_{2}}}{R} - I_{1} - I_{C} \sin(\phi), \\ C_{2} \frac{dV_{C_{2}}}{dt} = \frac{V_{C_{2}} - V_{C_{1}}}{R} - I_{2} + I_{C} \sin(\phi), \\ \frac{d\phi}{dt} = \frac{2e}{\hbar} \left(V_{C_{1}} - V_{C_{2}} \right). \end{cases}$$

$$(3)$$

$$L_{1} (m = 1, 2) \text{ denotes the current flowing through induced}$$

Here, I_m (m=1,2) denotes the current flowing through inductors L_m , while V_{C_n} (n=1,2) are the voltages across the capacitors C_n . It is worth mentioning that except for the JJ, all other circuit elements in Fig. 1 are assumed linear. The phase variation of the JJ element in Eq. (2) introduces a fifth state variable, turning the state equations from four to five.

By considering the following dimensionless states and variables, $t = \tau \sqrt{L_1 C_1}$, $\rho = \sqrt{L_1 / C_1}$, $x_1 = I_1 / I_C$, $x_2 = I_2 / I_C$, $x_3 = V_{C_1} / (\rho I_C)$, $x_4 = V_{C_2} / (\rho I_C)$, $x_5 = \phi$, $\alpha = \rho / R$, $\varepsilon_1 = L_1 / L_2$, $\varepsilon_2 = C_1 / C_2$, $\omega_0 = 2eI_C L_1 / \hbar$, we can write Eq. (3) as

$$\begin{cases} \dot{x_1} = x_3, \\ \dot{x_2} = \varepsilon_1 x_4, \\ \dot{x_3} = \alpha(x_3 - x_4) - x_1 - \sin(x_5), \\ \dot{x_4} = \varepsilon_2 \left(\sin(x_5) + \alpha(x_4 - x_3) - x_2\right), \\ \dot{x_5} = \omega_0(x_3 - x_4), \end{cases}$$
(4)

where α , ε_1 , ε_2 , and ω_0 are all positive parameters representing the ratio of resistors, inductances, and capacitors, respectively. The system of five interconnected differential equations [see Eq. (4)], representing the circuit model, is smooth and nonlinear. The sine function is the only nonlinear function in the model, and it involves only one state variable (namely, x_5).

C. System (4) properties: Phase space volume, symmetry, and steady states

Let us consider the dynamical system $\dot{X} = \Phi(X)$, where $X = (x_1, x_2, x_3, x_4, x_5)^T$ and $\Phi(X) = (\phi_1(X), \phi_2(X), \phi_3(X), \phi_4(X), \phi_5(X))^T$. From the theory, the volume contraction/expansion rate is given by the following Lie derivative:

$$\Lambda = \nabla \cdot \Phi(X) = \frac{\partial \phi_1}{\partial x_1} + \frac{\partial \phi_2}{\partial x_2} + \frac{\partial \phi_3}{\partial x_3} + \frac{\partial \phi_4}{\partial x_4} + \frac{\partial \phi_5}{\partial x_5}.$$
 (5)

After straightforward calculations on system (4), the volume contraction/expansion rate yields

$$\Lambda = \alpha (1 + \varepsilon_2). \tag{6}$$

Given that α and ε_2 are positive parameters, the volume Λ is, therefore, expanding making the system in Eq. (4) to be non-dissipative. In other words, the system's trajectories contained in the volume V at the time $t \to 0$ will abruptly increase as time progress toward infinity [i.e., $V(t) = V(0) \exp{\{\Lambda t\}}$]. Thus, system (4) is volume expanding around the steady states.

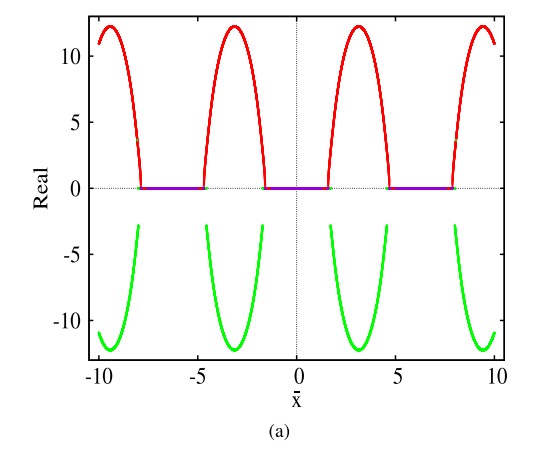
It is worth recalling that the property of involutional symmetry in dynamical systems consists of not altering the dynamical equations when one or more of the variables changes sign. According to the relevant work of Ref. 38, basic involutional symmetries, such as inversion, rotation, and reflection, are involved. System (4) is found to be inversion invariant since their dynamical equations remain unchanged when the coordinates are substituted with their negation. This means that the results of system (4) will either appear as individual symmetric solutions or in pairs that exhibit symmetry in order to match the inversion invariance property of the dynamical equations. This property is significant when examining coexisting solutions through symmetry breaking or restoring crisis.

It is known that the steady states play an essential role in the characterization of dynamical systems. 50,51 They are calculated by setting the left-hand side of Eq. (4) to zero; this yields

$$\begin{cases} \bar{x}_3 = \bar{x}_4 = 0, \\ \bar{x}_2 = -\bar{x}_1 = \sin(\bar{x}_5). \end{cases}$$
 (7)

From Eq. (7), two scenarios are observed:

- $\forall (\bar{x}_1, \bar{x}_2) \notin [-1, 1]$, system (4) has no equilibrium points and one may observe hidden dynamics^{52,53} and
- $\forall (\bar{x}_1, \bar{x}_2) \in [-1, 1]$, system (4) has an infinite number of steady state in the space (x_1, x_2, x_5) .



From the second hypothesis, we have derived in Eq. (8) the Jacobean matrix of system (4),

$$M_{J} = \begin{bmatrix} 0 & 0 & 1 & 0 & 0 \\ 0 & 0 & 0 & \varepsilon_{1} & 0 \\ -1 & 0 & \alpha & -\alpha & -\cos(\bar{x}_{5}) \\ 0 & -\varepsilon_{2} & -\alpha\varepsilon_{2} & \alpha\varepsilon_{2} & \varepsilon_{2}\cos(\bar{x}_{5}) \\ 0 & 0 & \omega_{0} & -\omega_{0} & 0 \end{bmatrix}.$$
(8)

The characteristic equation associated with Eq. (8) is given by

$$|M_I - \xi I_5| = c_5 \xi^5 + c_4 \xi^4 + c_3 \xi^3 + c_2 \xi^2 + c_1 \xi + c_0, \tag{9}$$

where I_5 is a 5×5 identity matrix. The coefficients c_i (with i = 0, ..., 5) are defined as $c_5 = 1$, $c_4 = -\alpha(\varepsilon_2 + 1)$, $c_3 = \varepsilon_2(\alpha)$ $+\omega_0\cos(\bar{x}_5)$, $c_2=-\alpha\varepsilon_2\omega_0\cos(\bar{x}_5)$, $c_1=c_0=0$. The eigenvalues ξ_i (i = 1, 2, 3, 4, 5) corresponding to Eq. (9) are obtained by varying $\bar{x_5}$ over certain range and fixing the values of the other system parameters. The eigenvalues obtained for the parameters $\varepsilon_1 = 15$, $\varepsilon_2 = 3.8596, \, \omega_0 = 39.6529, \, \alpha = 1.7408 \times 10^{-5}$ (corresponding to a four-scroll attractor discussed in Sec. III) are shown in Fig. 2. The eigenvalues ξ_1, ξ_2 are observed to be real and unequal or a pair of complex conjugates with variation in \bar{x} , while the eigenvalue ξ_3 is always zero. The eigenvalues ξ_4, ξ_5 are a pair of complex conjugates with positive real parts for all values of \bar{x}_5 . Hence, the fixed point corresponding to a value of \bar{x}_5 is an unstable saddle-focus, leading to the expansion of phase space of the system along the \bar{x}_5 -axis. Figures 2(a) and 2(b) show the variation of the real parts of the eigenvalues ξ_1, ξ_2 and ξ_4, ξ_5 with \bar{x}_5 , respectively.

III. COMPUTATIONAL INVESTIGATIONS

A. Numerical schemes

Numerical approaches involve the use of the fourth-order Runge–Kutta algorithm implemented in C++. The integration steps are always fixed at $\Delta \tau \leq 10^{-3}$, and the system parameters and variables are set in a double format. Unless explicitly mentioned, long transients of 30 000 data points of integration are always discarded.

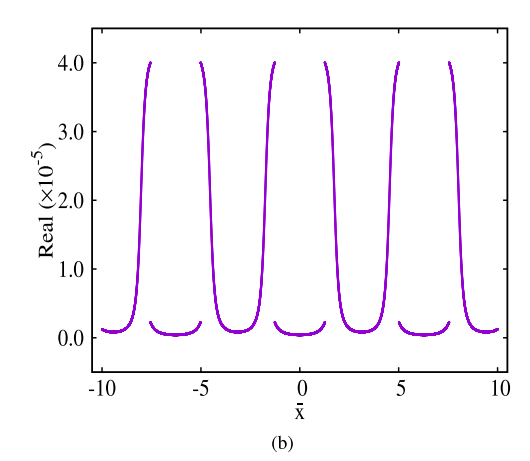


FIG. 2. Eigenvalues of Eq. (9) as a function of \bar{x}_5 . (a) Real parts of eigenvalues ξ_1 (red), ξ_2 (green), and the real part of the complex conjugates of ξ_1 , ξ_2 (violet) indicating the saddle nature of corresponding \bar{x} . (b) The real part of complex conjugates of the eigenvalues ξ_4 , ξ_5 representing the unstable focus behavior.

Both qualitative and quantitative tools, such as bifurcation diagrams, the spectrum of Lyapunov exponents, phase portraits, and time series, are used to reveal the bifurcation scenarios, multi-scrolls, and homogeneous and heterogeneous multistability in the system (4). For the bifurcation analysis, the parallel bifurcation method is exploited. It involves superimposing various sets of data obtained by recording extrema of the nonlinear system with fixed initial conditions at each step of the control parameter. The graphs of the Lyapunov exponent spectrum are obtained using the algorithm of Wolf *et al.*⁵⁴

B. Complex patterns, multi-scrolls, and transitions to chaos

The behavior of system (4) is analyzed by studying the impact of parameters on its dynamics in order to observe the complex patterns it can generate. Figure 3 displays the phase portraits in the (x_5, x_4) plane for specific values of α , ε_1 , and ε_2 . These phase portraits reveal a variety of complex patterns and dynamics, including multi-scroll chaotic attractors and quasiperiodic oscillations in both

2D and 3D. To gain a better understanding of the system's sensitivity to the control parameter α , we present in Figs. 4(a) and 4(b), respectively, the bifurcation diagram and the spectrum of Lyapunov exponents with the set of parameters of Fig. 3(b). In Fig. 4(a), three sets of data are overlaid on the bifurcation diagram, each obtained by reinitializing the initial conditions at each step of the control parameter. The diagram in green color represents the solution of system (4) with fixed initial conditions (0, -0.7, 0.3, 0, 1), while those in black and red colors correspond to fixed initial conditions (0, -1.0, -0.2, 0, 0) and (0, 0.7, 0.2, 0, 0), respectively. It is evident that these three sets of data do not perfectly overlap, indicating the presence of multistability in system (4). Additionally, some of the bifurcation diagrams in Fig. 4(a) exhibit stratification or layering for certain initial conditions (black and green curves), coexisting with the more compact red curve within a specific range of the control parameter. These stratifications support the occurrence of multi-scroll behaviors within the investigated system.31 Those stairs/layers (i.e., multi-scrolls) are varying with α . Further insights on the dynamical evolution of system (4) are observed through the 3D phase diagrams in Fig. 5 where seven attractors are

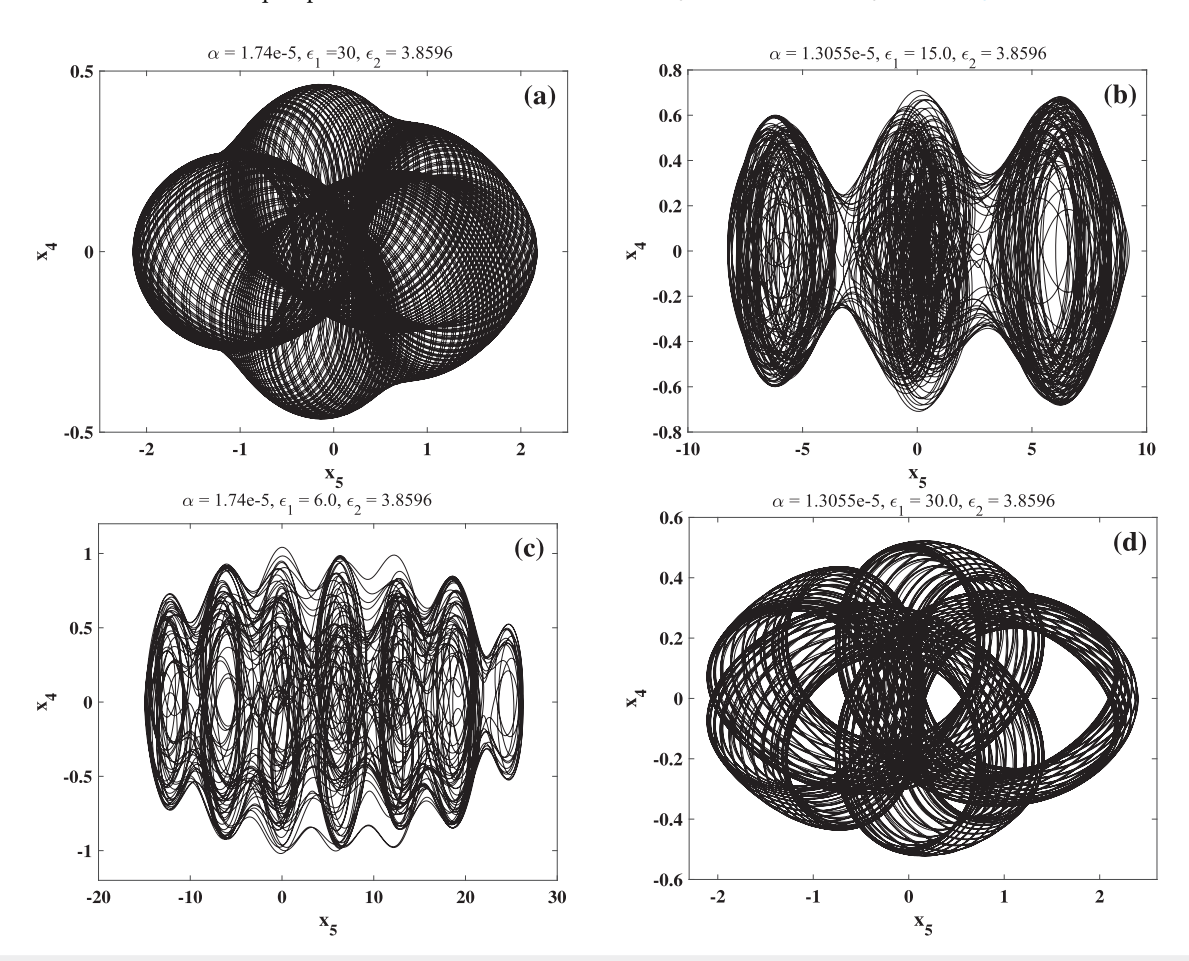
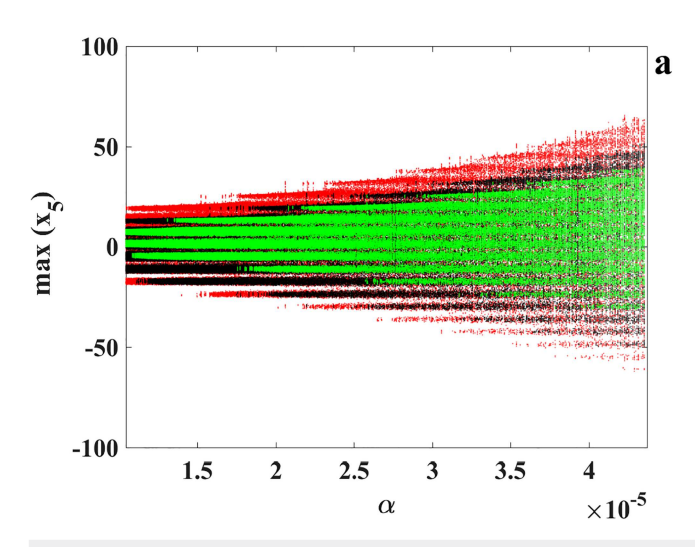


FIG. 3. Phase diagrams of system (4) in the plane (x_5, x_4) for specific parameter values α , ε_1 , ε_2 , and $\omega_0 = 39.6529$. (a) 3D torus, (b) three-scroll chaotic attractor, (c) seven-scroll chaotic attractor, and (d) 2D torus. The initial conditions are (0, 0.7, 0.2, 0, 0).



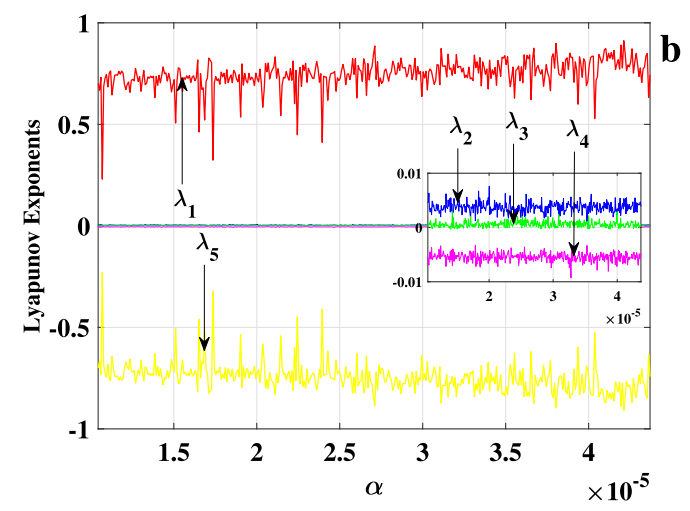


FIG. 4. (a) Bifurcation diagrams showing the local maxima of the state variable $x_5(\tau)$ when varying the control parameter $\alpha \in [1.044, 4.37] \times 10^{-5}$. Three sets of data obtained from computing the system using different initial conditions are superimposed by exploiting the parallel bifurcation technique⁴⁰ (refer to the main text for details). (b) The corresponding spectrum of the five Lyapunov exponents of system (4) vs α . Other parameters were fixed as $\varepsilon_1 = 15.0$, $\varepsilon_2 = 3.8596$, and $\omega_0 = 39.6529$.

depicted when tunning α . The figure clearly demonstrates the presence of various multi-scroll attractors in the phase space (x_5, x_4) ; for instance, when $\alpha = 9.3256 \times 10^{-6}$, the system is quasiperiodic (see attractor A_1 in Fig. 5). When selecting discrete values of α in $[1.044, 4.37] \times 10^{-6}$, system (4) undergoes 2-scroll, 3-scroll, 4-scroll, and up to 12-scroll chaotic dynamics (see attractors A_2 – A_7 of Fig. 5).

It is worth mentioning that the volume expanding property of system (4) is clearly confirmed along each axes of Fig. 5 when increasing, respectively, α and ε_2 (although not discussed in this paper for consistency). Moreover, the fact that system (4) is of inversion invariant type and has no or infinite equilibria (as discussed in Sec. II C) further emphasizes the extreme multistability experienced by the system.

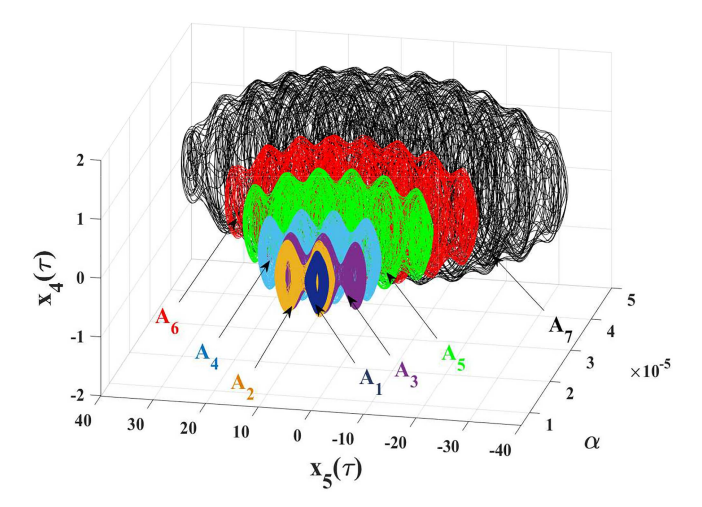


FIG. 5. Numerical 3D phase spaces of system (4) for seven selected values of the parameter α , illustrating the variation in the number of scrolls. Torus for $\alpha=9.3256\times 10^{-6}$ (A_1), 2-scroll for $\alpha=1.0445\times 10^{-5}$ (A_2), 3-scroll for $\alpha=1.2145\times 10^{-5}$ (A_3), 4-scroll for $\alpha=1.7408\times 10^{-5}$ (A_4), 6-scroll for $\alpha=2.6112\times 10^{-5}$ (A_5), 8-scroll for $\alpha=3.264\times 10^{-5}$ (A_6), and 12-scroll for $\alpha=4.3519\times 10^{-5}$ (A_7). The initial states were fixed as $X(0)=(0,0.7,0.2,0,0)^T$.

IV. HETEROGENEOUS EXTREME MULTISTABILITY WITH MULTI-SCROLLS

Heterogeneous multistability is defined as the coexistence of different patterns/attractors when varying solely the initial conditions with fixed parameters. One effective tool used in the analysis is the bifurcation diagram of initial conditions, which helps in addressing the number of coexisting attractors arising from hysteresis and parallel bifurcation branches. 40,55 In Fig. 6, a map of the twoparameter Lyapunov exponent for $-50 \le x_5(0) \le 50$ and $1 \le \alpha$ ≤ 1.45 is illustrated. A noticeable transition of dynamics from chaotic oscillations, marked by yellow-reddish color, to quasiperiodic states in black color occurs for fixed values of α with varying initial condition $x_5(0)$. It is observed that regions of quasiperiodic dynamics (in black color) become narrower as the value of α increases. To further comprehend the qualitative dynamics, Fig. 7(a) exhibits the bifurcation diagram of the maxima of x_1 vs the initial state $x_2(0)$. As the investigated system is inversion invariant, the bifurcation diagram exhibits symmetry over the origin. This indicates that attractors appear in symmetric pairs to restore the system's exact symmetry. Two qualitative dynamics, chaos, and 2D/3D quasiperiodic oscillations are also observed [see Fig. 7(a)]. This is corroborated through the spectrum of Lyapunov exponents in Fig. 7(b), where regions with one positive Lyapunov exponent represent chaotic behavior, while those with two or three zero Lyapunov

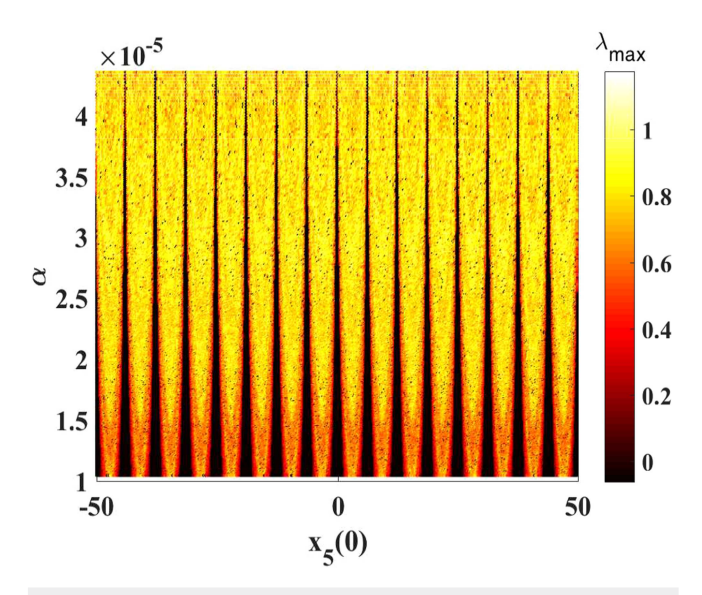


FIG. 6. 2D map of the Lyapunov exponent in the plane $[x_5(0),\alpha]$ highlighting the heterogeneous multistability in system (4). Black regions mark the quasiperiodic dynamics, while the yellow-reddish regions are those of chaotic oscillations.

exponents depict quasiperiodic dynamics. The volume expanding property is also visible in the bifurcation diagram of Fig. 7(a). The results in Fig. 7 are obtained by fixing $\alpha = 1.3056 \times 10^{-5}$ and selecting initial states as $[x_1(0), x_3(0), x_4(0), x_5(0)] = (0, 0.2, 0, 0)$.

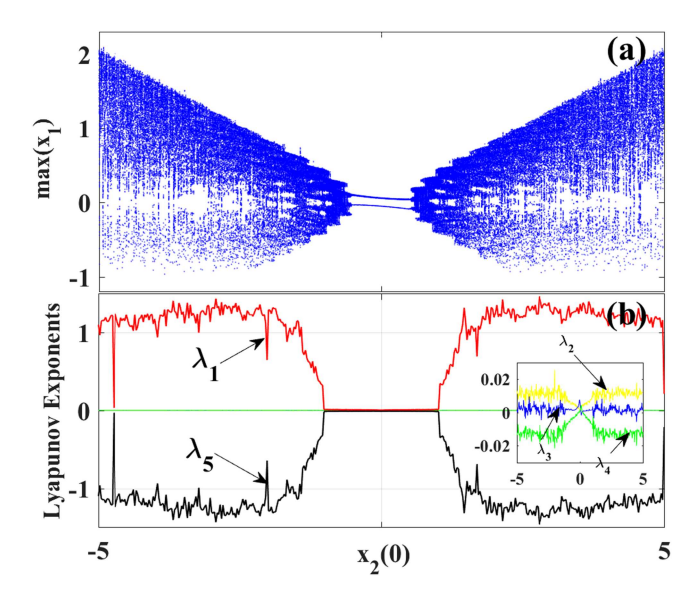


FIG. 7. (a) Bifurcation diagram of system (4) illustrating the local maxima of $x_1(\tau)$, accompanied by the corresponding (b) spectrum of Lyapunov exponents vs the initial state $x_2(0)$ for $\alpha=1.3056\times 10^{-5}$. Qualitative changes in both diagrams indicate the system experiencing the phenomenon of extreme multistability. The other initial conditions were fixed as $[x_1(0), x_3(0), x_4(0), x_5(0)] = (0, 0.2, 0, 0)$.

By choosing symmetric initial conditions as depicted in Fig. 8, the phenomenon of heterogeneous extreme multistability is vividly highlighted through various phase portraits. These include pairs of symmetric chaotic multi-scroll attractors [see Figs. 8(a)–8(e)], quasiperiodic attractors [see Figs. 8(f) and 8(f)], and symmetric chaotic attractors [see Figs. 8(g) and 8(h)]. Clearly, different dynamical topologies were captured by varying solely the initial states with fixed control parameter α . It is also noteworthy that the initial conditions induce multi-scroll selection, as highlighted in Figs. 8(a)–8(e).

V. HOMOGENEOUS EXTREME MULTISTABILITY AND INITIAL OFFSET BOOSTING

In contrast to offset boosting, which involves the utilization of an additive constant to switch between bipolar and unipolar signals by introducing additional electronic components as accessible state parameters, 56,57 the results presented here are more relevant in two senses:

- System (4) is capable of self-generating initial offset boosting with coexistence of infinitely many attractors⁵⁸ and
- Homogeneous extreme multistability with any number of scrolls is also achievable by fixing α and then varying the initial states.

It is important to recall that homogeneous multistability represents the system's capacity to exhibit qualitative similar coexisting solutions shifted in the state space solely by varying initial states.⁵⁵ In system (4) by fixing the initial state $x_5(0)$ to $\frac{\pi}{2} \pm k2\pi$ ($k \in \mathbb{Z}$) while setting all others to zero, we have effectively captured the phenomenon of homogeneous multistability. This is clearly evident in the bifurcation diagram of Fig. 9(a) where infinite, uniform, and symmetric layer band patterns are observed on each other side of the origin $x_5(0) = 0$. This bifurcation diagram aligns perfectly with the spectrum of Lyapunov exponents depicted in Fig. 9(b). It is worth mentioning that the repeated layered patterns observed in the bifurcation diagram of Fig. 9(a) demonstrate that some of coexisting heterogeneous solutions are of multi-scrolls type. This is clearly illustrated in Fig. 10 by the phase portraits showing the coexistence of 4-scrolls in the phase space (x_5, x_4) for different symmetric initial conditions; for instance, with $x_5(0) = \pm \pi/2$, a pair of symmetric chaotic 4-scroll attractors are obtained in Fig. 10(a). By fixing $x_5(0) = \pm 21\pi/2$, the attractors shift away from each other, and the centers of their manifolds are separated by 21π [see Fig. 10(e)]. Henceforth, we can generalize that when selecting $x_5(0)$ in the form of $\frac{\pi}{2} \pm k2\pi$ ($k \in \mathbb{Z}$), initial offset boosting can be observed along the x_5 -axis while preserving the intrinsic dynamics (i.e., 4-scrolls).

Although still exhibiting heterogeneous extreme multistability, the selection of only positive or negative initial conditions leads to the generation of homogeneous extreme multistability, as depicted in Fig. 11. Indeed, the first five attractors displaying the same characteristics but shifted in the state space are depicted in Figs. 11(a) and 11(b). The offset statistical property is used to track the demarcation region of initial state for each coexisting solutions as presented in Fig. 11(c). In that diagram, the colors are associated with each coexisting attractor in Figs. 11(a) and 11(b), while the white color represents other untracked dynamics. The phenomenon of homogeneous extreme multistability discussed here is

30 May 2024 15:44:56

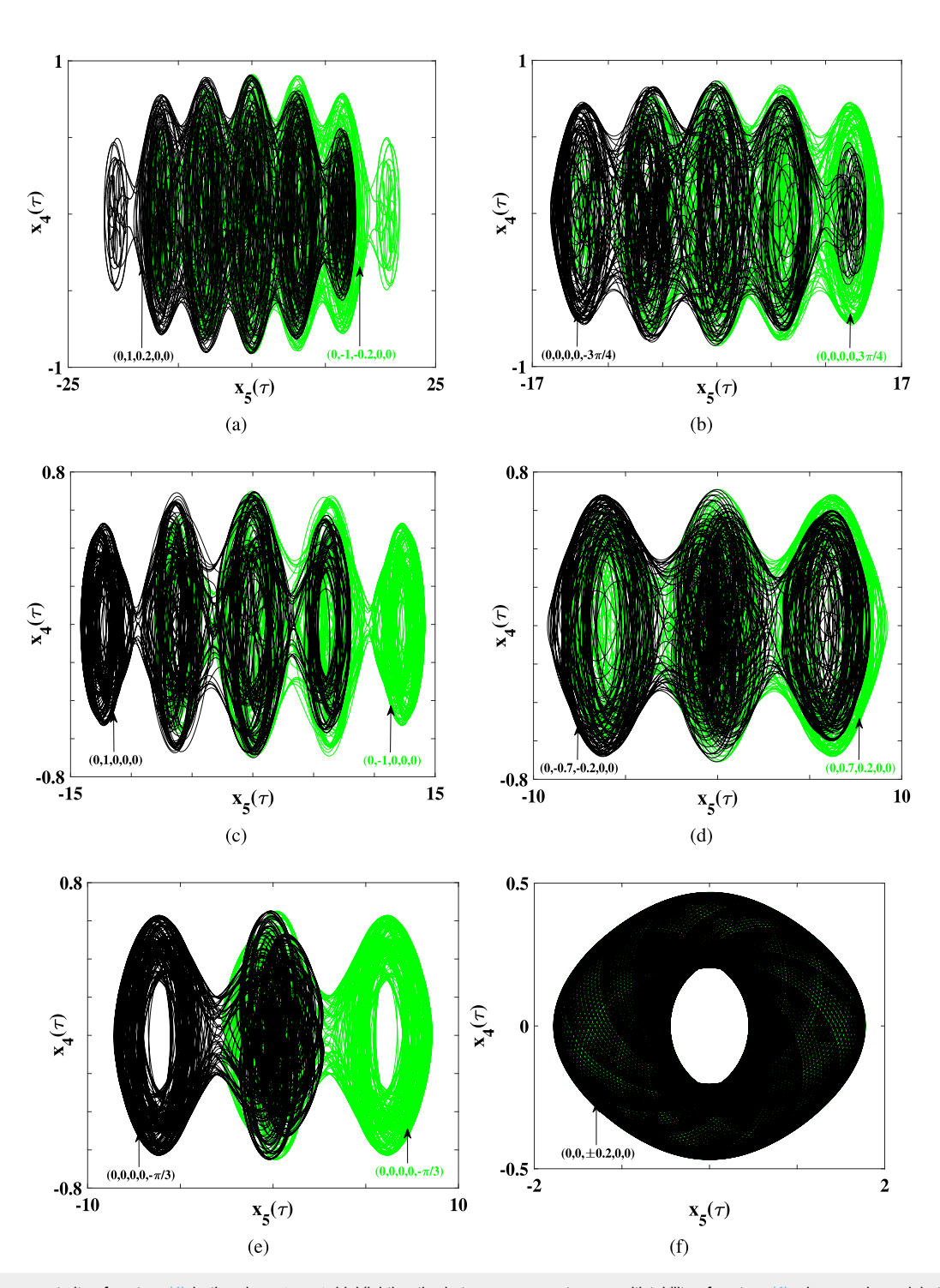


FIG. 8. 2D phase portraits of system (4) in the plane (x_5, x_4) highlighting the heterogeneous extreme multistability of system (4) when varying solely the initial conditions as depicted in the diagrams with a fixed control parameter $\alpha=1.3056\times 10^{-5}$. (a) Symmetric 6-scroll for $X(0)=(0,\pm 1,\pm 0.2,0,0)$, (b) symmetric 5-scroll for $X(0)=(0,0,0,0,\mp 3\pi/4)$, (c) symmetric 4-scroll for $X(0)=(0,\pm 1,0,0,0)$, (d) symmetric 3-scroll for $X(0)=(0,\pm 0.7,\pm 0.2,0,0)$, (e) symmetric 2-scroll for $X(0)=(0,0,0,0,\pm 0.2,0,0)$, (f) quasiperiodic attractor for $X(0)=(0,\pm 0.2,0,0,0)$, (g) symmetric chaotic attractors for $X(0)=(0,\pm 3,\pm 1.2,0,0)$, (i) chaotic attractors for $X(0)=(0,\pm 0.1,\pm 1.2,0,0)$, and (j) quasiperiodic attractor for $X(0)=(0,0,0,0,\pm 0.2,0)$.

30 May 2024 15:44:56

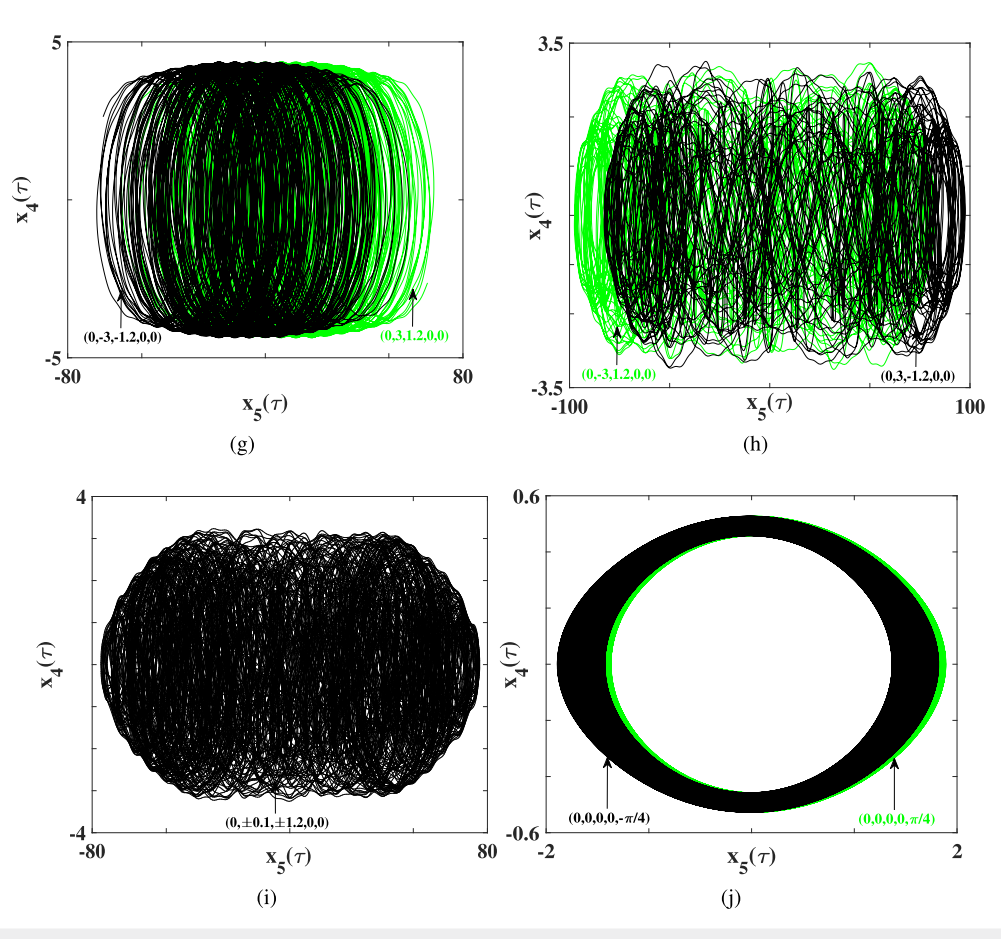


FIG. 8. (Contineud.)

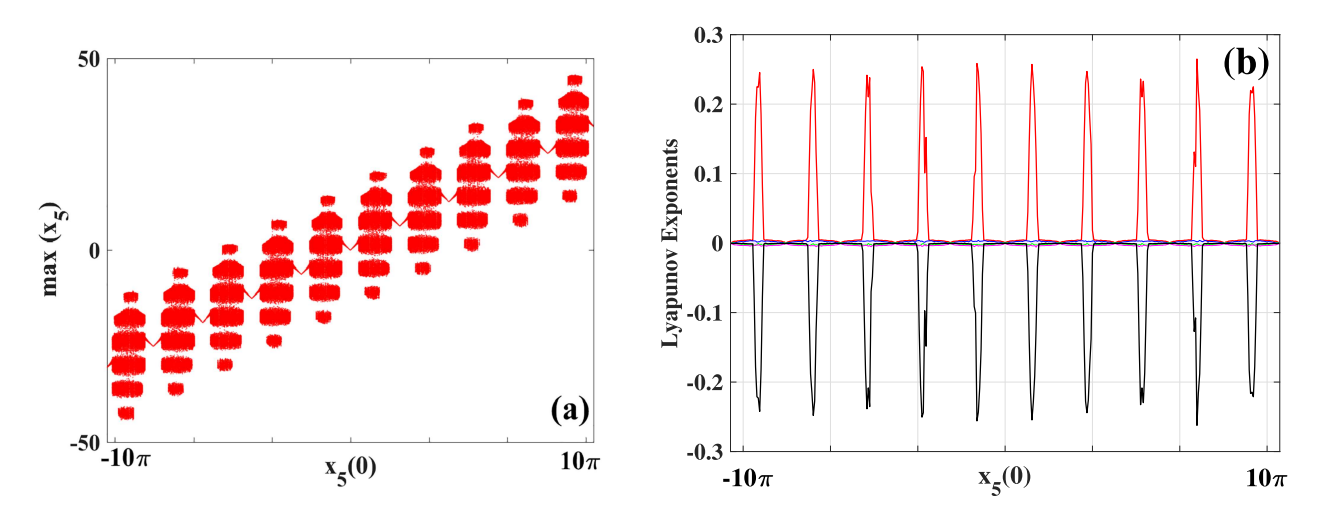


FIG. 9. (a) Bifurcation diagram of initial conditions showing the maxima of x_5 in the form of layered band patterns highlighting homogeneous and heterogeneous multi-scrolls in system (4) as a function of the initial condition $x_5(0) \in [-10\pi, 10\pi]$ with all other ones set at zero. (b) Corresponding spectrum of Lyapunov exponents. The control parameter is fixed as $\alpha = 1.3056 \times 10^{-5}$.

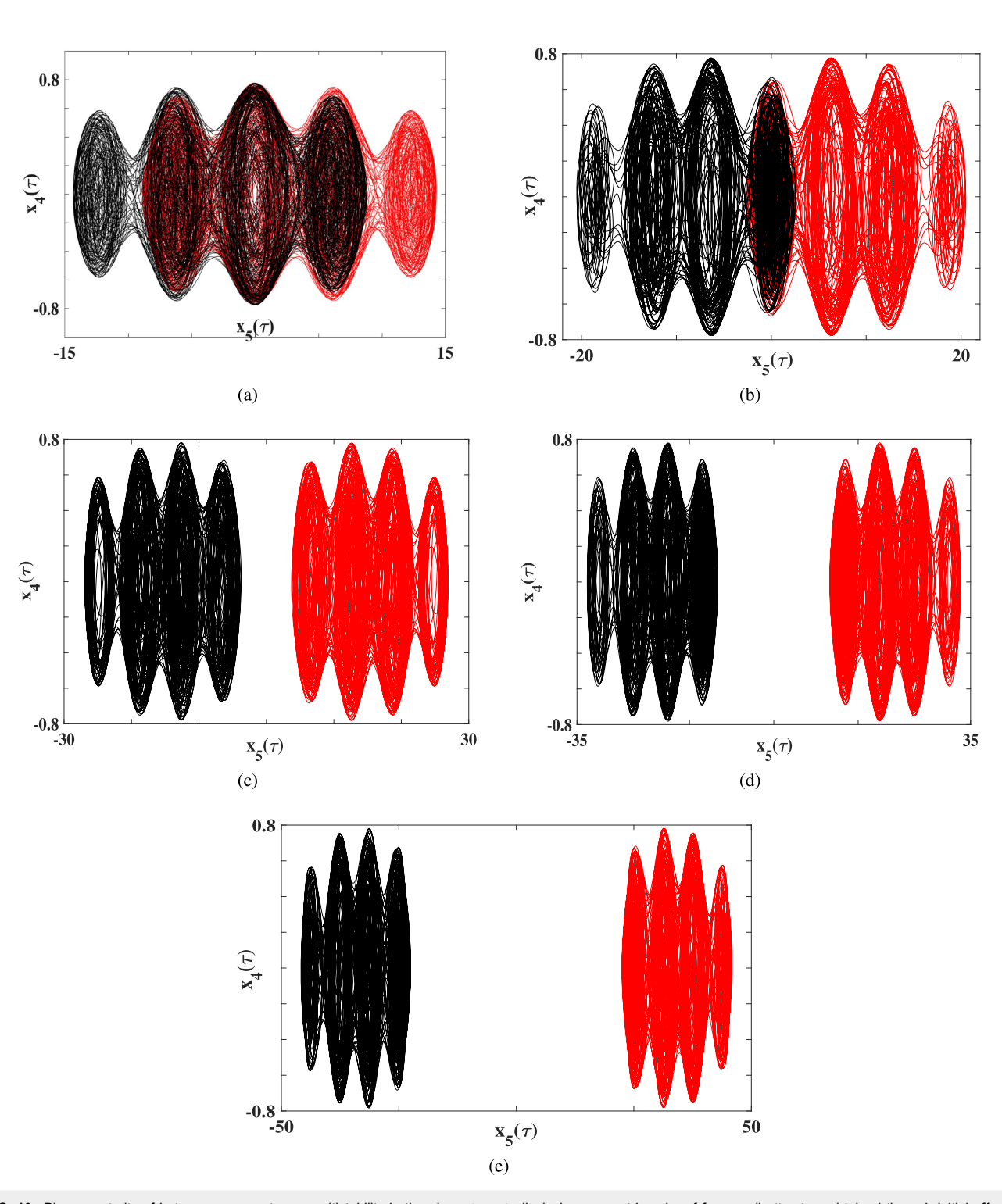


FIG. 10. Phase portraits of heterogeneous extreme multistability in the plane (x_5, x_4) displaying symmetric pairs of four-scroll attractors obtained through initial offsets in the phase space and for the fixed control parameter $\alpha=1.3056\times 10^{-5}$. (a) $x_5(0)=\pm\pi/2$, (b) $x_5(0)=\pm5\pi/2$, (c) $x_5(0)=\pm9\pi/2$, (d) $x_5(0)=\pm13\pi/2$, and (e) $x_5(0)=\pm21\pi/2$. When selecting only positive or negative signs of the initial state $x_5(0)$, homogeneous multistability is captured, as depicted in Fig. 11.

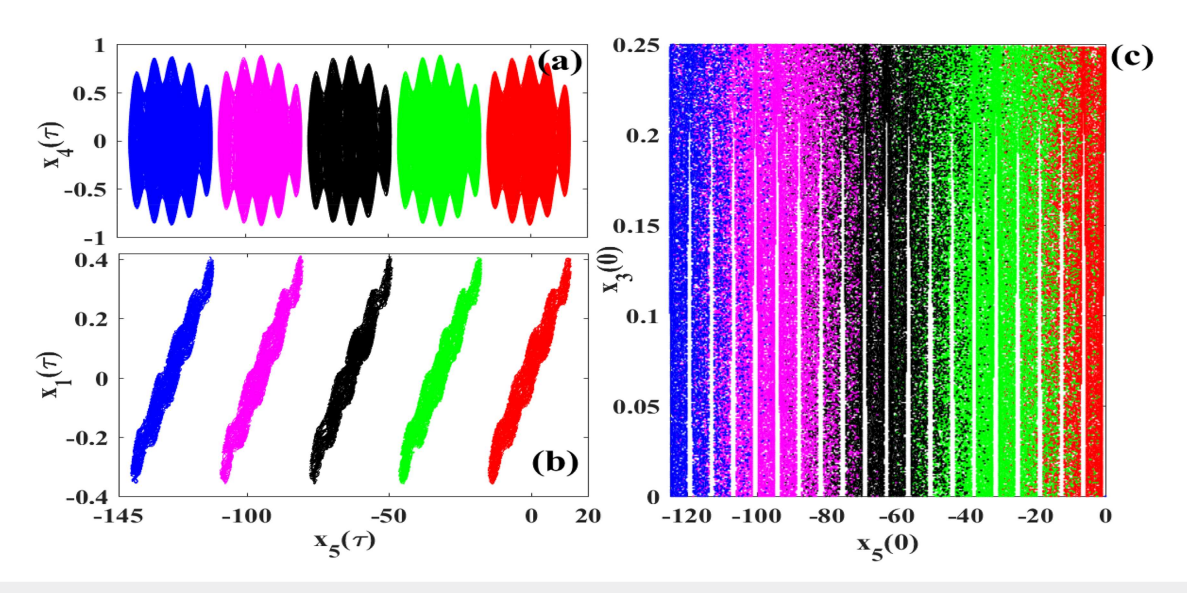


FIG. 11. (a) Phase portraits of five scrolls in the plane (x_5, x_4) and (b) in the plane (x_5, x_1) . Additionally, (c) denotes the demarcation region of each coexisting attractor in the plane $[x_5(0), x_3(0)]$, supporting homogeneous extreme multistability. Five attractors are plotted for five distinct initial states $X(0) = [0, 0.7, 0.2, 0, x_5(0)]^T$ and with $\alpha = 1.684 62 \times 10^{-5}$. The color label and the initial state for each attractor are as follows: red color for $x_5(0) = -\pi/2$, green color for $x_5(0) = -21\pi/2$, black color for $x_5(0) = -41\pi/2$, magenta color for $x_5(0) = -61\pi/2$, and blue color for $x_5(0) = -81\pi/2$.

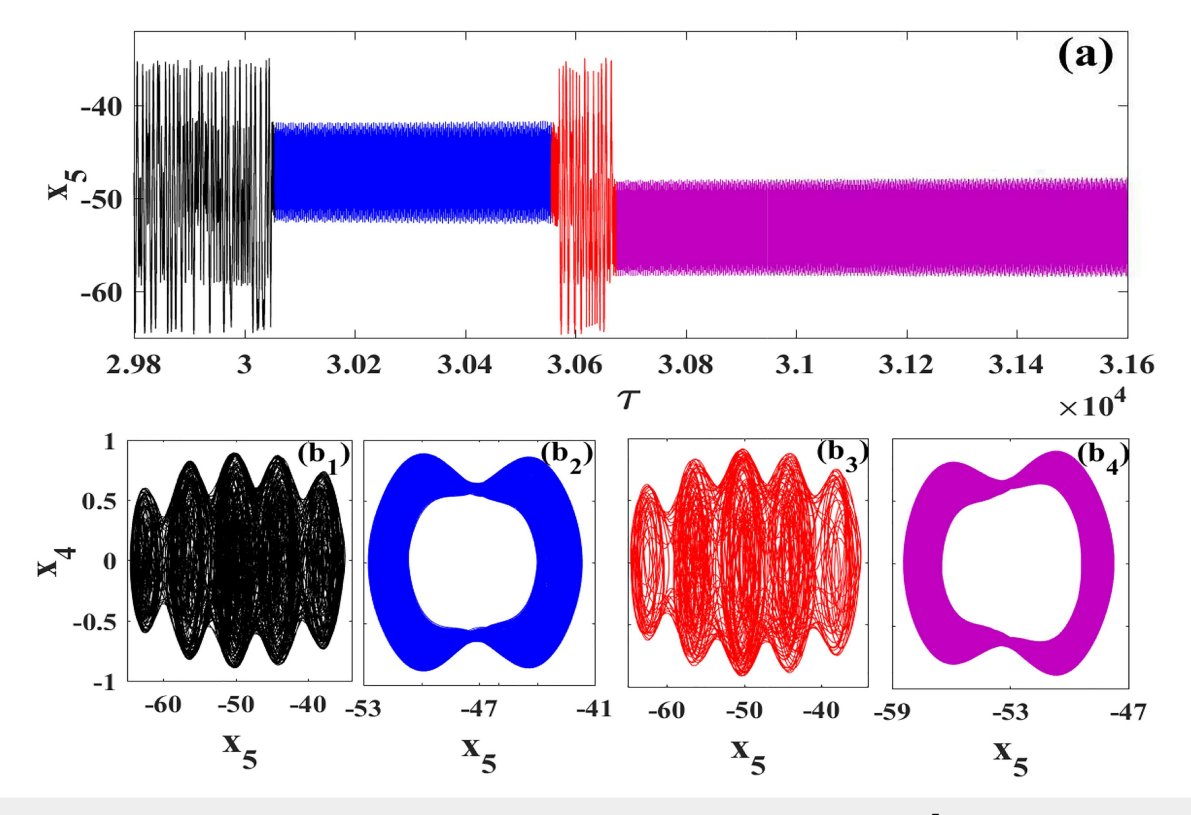


FIG. 12. Multi-metastable phenomenon in system (4) for $\alpha = 1.7408 \times 10^{-5}$ and initial conditions $X(0) = (0, 0, 0, 0, -31\pi/2)^T$. (a) Time trace of the variable $x_5(\tau)$ and (b) phase portraits at different time intervals. (b1) Depicts chaos with five scrolls, (b2) single-band chaos, (b3) chaos with five scrolls, and (b4) single-band chaos.

FIG. 13. Finite-time Lyapunov exponent spectra $(\lambda_{1,2,3,4})$ showing the transition from a transient to permanent regime. Parameters and initial conditions are those of Fig. 12.

of high interest in engineering applications requiring only unipolar signals. 60

VI. MULTI-METASTABLE DYNAMICS

Metastability or transient chaos is a phenomenon wherein trajectories, originating from a variety of randomly chosen initial states, initially exhibit chaotic behavior over an extended period before abruptly or gradually evolving into a final attractor, often of a nonchaotic nature.⁶¹ Recent investigations have revealed instances of

Arduino IDE

USB Cable connector

TFT 3.5 Inch LCD display connected on top of an Arduino Mega 2560

PC

double and tri-transient chaos in both integer and fractional order systems.^{62,63} Moreover, it is noteworthy that several studies have underscored the heightened significance of this transient behavior for various applications.^{64–66}

By fixing the system parameters to $\alpha = 1.7408 \times 10^{-5}$, $\varepsilon_1 = 15.0$, $\varepsilon_2 = 3.8596$, $\omega_0 = 39.6529$ and initial conditions as $(0,0,0,0,-31\pi/2)$, the time series in Fig. 12(a) illustrates the tritransient chaotic behaviors. Each motion state in the time series is represented with a different color, and a correlation is detected with the phase diagrams in Fig. 12(b). As it can be observed in Fig. 12, the first and third transient regimes are chaotic and characterized by five scrolls, as depicted in Figs. 12(b1) and 12(b3), respectively. In contrast, the second transient regime, captured in Fig. 12(b2), displays a single-band chaotic dynamic. The persistent dynamical behavior of the system following these transients represents another single-band chaotic behavior, as plotted in Fig. 12(b4). The tri-transient feature is further validated by the finite-time Lyapunov exponent (FTLE) spectra as depicted in Fig. 13. Unlike qualitative tools, such as phase portraits and time series, the FTLE provides a statistical measure of the extent to which a trajectory stretches or folds in a specific direction within a defined interval. 67 The FTLE is evaluated as

$$\lambda_j^{\overline{m}} = \frac{1}{m} \sum_{i=1}^M \lambda_j^m, \qquad m = 1, 2, \dots, k,$$
(10)

where M denotes the time interval and λ_j^m is the instantaneous Lyapunov exponents, which is defined as

$$\lambda_i^m = \log \|e_i^m\|. \tag{11}$$

The reorthonormalization vector e_i^m is denoted as

$$e_i^m = M_I(x_j, y_j, \Theta_j, \phi_j) \hat{e}_i^m.$$
 (12)

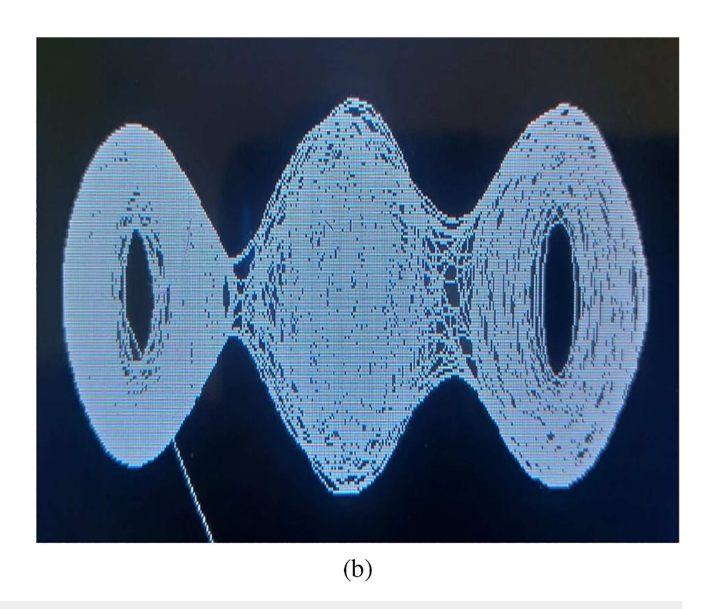


FIG. 14. (a) Microcontroller implementation for system (4) with an Arduino Mega 2560. (b) Phase portraits in the plane (x_5 , x_4) of a three-scroll chaotic oscillator display on the TFT 3.5 inch LCD screen.

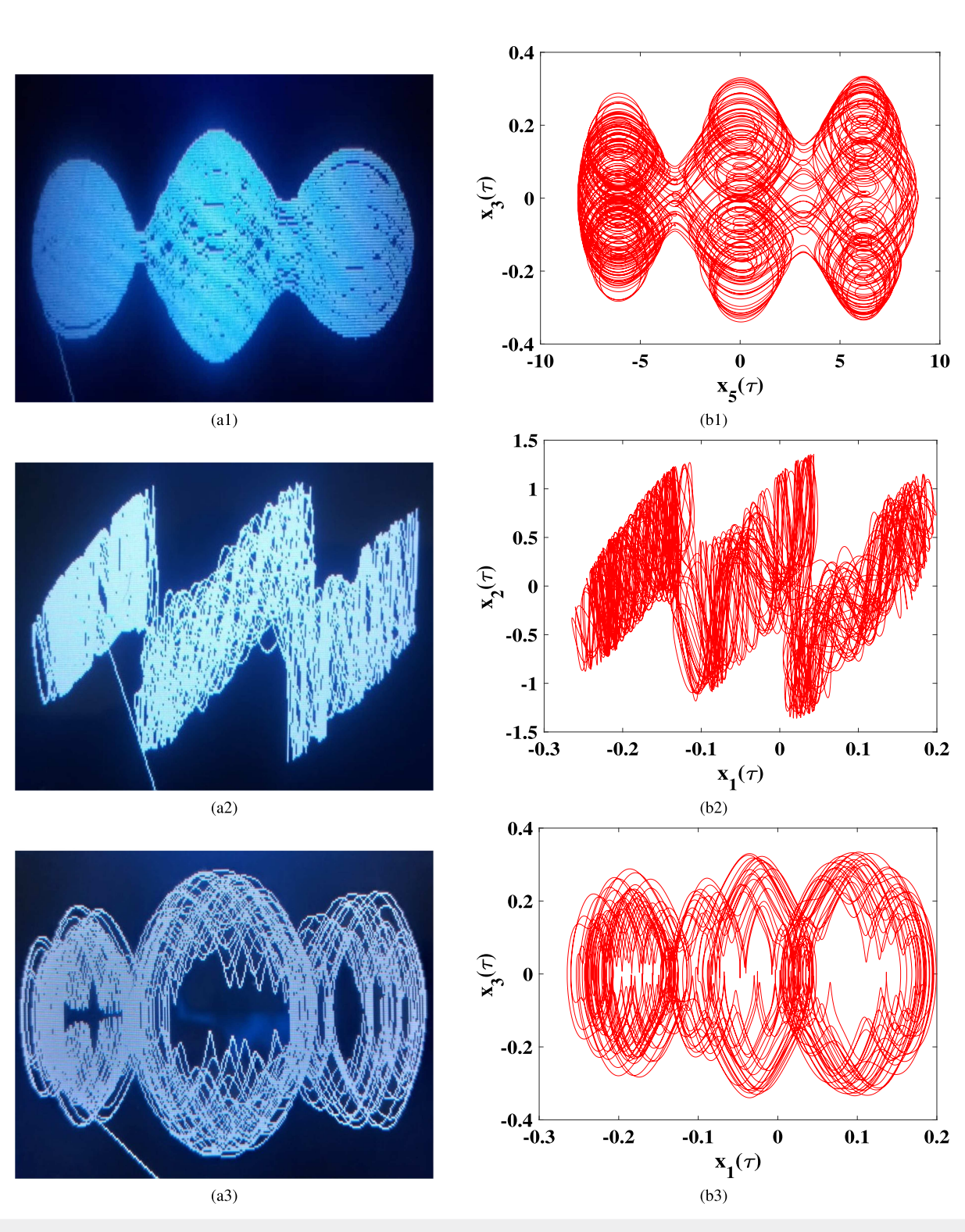


FIG. 15. (a1)–(a6) Experimental results and their (b1)–(b6) numerical equivalence of the three scrolls chaotic attractor in various phase spaces for $\alpha=1.2145\times 10^{-5}$, $\varepsilon_1=15.0, \varepsilon_2=3.8596, \omega_0=39.6529$ and initial conditions fixed at X(0)=(0,0.7,0.2,0,0).

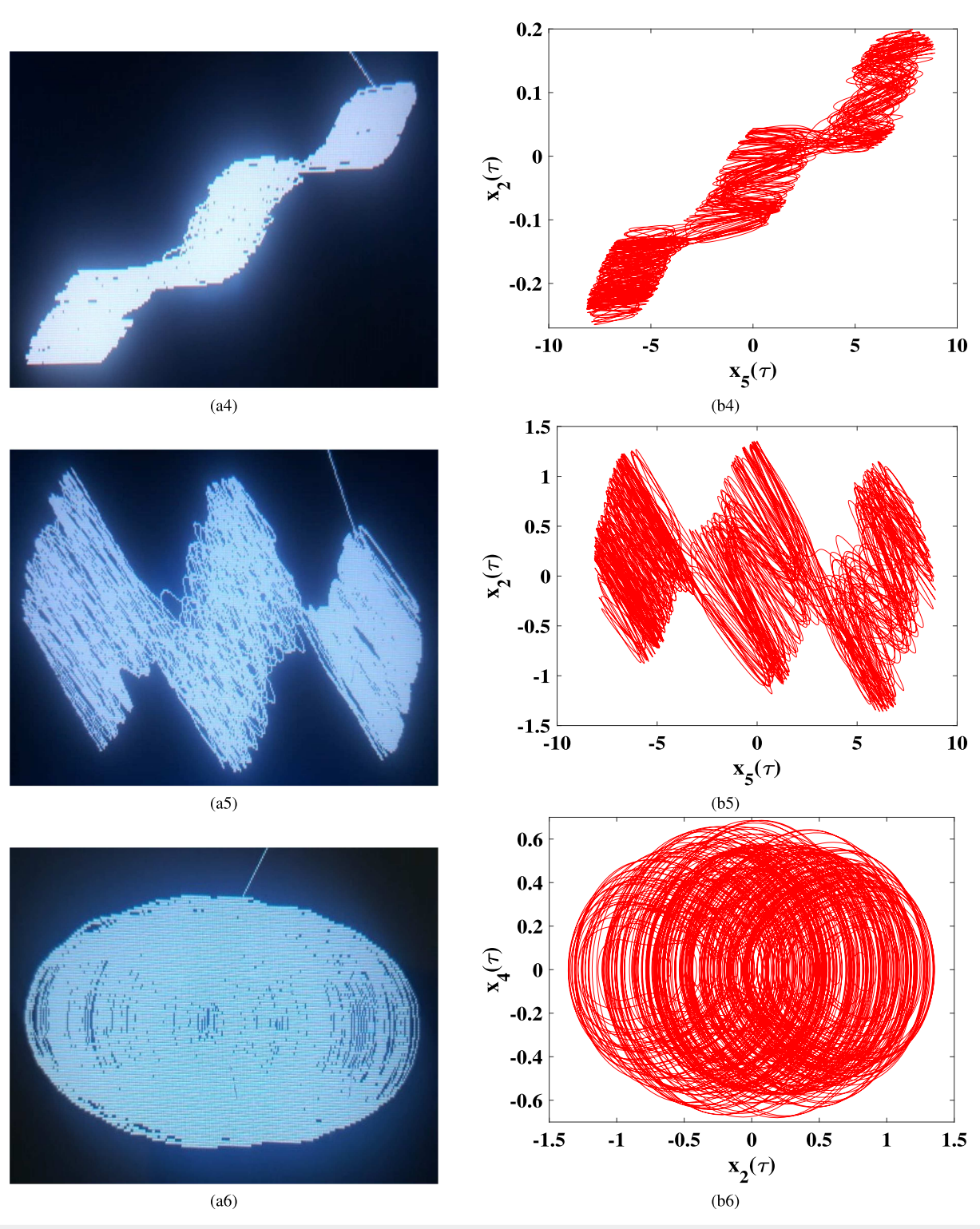


FIG. 15. (Continued.)

Here, M_J represents the Jacobean matrix in Eq. (8), and j refers to the time step. Figure 13 showcases the evolution of the time series Lyapunov exponent computed over M=200 data points with a step size of 0.005. One can notice in Fig. 13 the persistence of a positive Lyapunov exponent over the long-time run, confirming the chaotic nature of the system post the elimination of all transient regimes. In addition, the zoomed-in view in Fig. 13 reveals three rapid switches between two Lyapunov exponents (depicted in red and green colors) in the spectra. These switches are demonstrating the tri-transient dynamics captured in the investigated system.

VII. MICROCONTROLLER MEASUREMENTS

This section presents the microcontroller experimental kit used to capture phase portraits. It includes an Arduino Mega board equipped with an ATMega2560 microcontroller clocked at 16 MHz, a 32-bit data bus, flash memory, and 256 kB of SRAM, along with 8 kB of flash memory. The board features 54 input/output pins, while the firmware is developed using the Arduino IDE software. The computational results for system (4) are obtained by the fourthorder Runge-Kutta method. The phase portraits are displayed on a 3.5 inch GLCD screen with a resolution of 320 \times 480 and a 65 K color display. This setup is fully compatible with the ATMega2560 microcontroller and supports SD card expansion. It operates using 8-bit parallel communication and an ILI9486 driver. The complete experimental board is depicted in Fig. 14(a), showing the GLCD screen displaying a three-scroll chaotic oscillator as illustrated in Fig. 14(b). Figure 15 presents the experimental measurements in the left panel and their corresponding numerical equivalence from MATLAB in the right panel for $\alpha = 1.2145 \times 10^{-5}$. One can observe good agreement between both results.

VIII. CONCLUSION

In this paper, we have investigated the dynamics of coupled resonant circuits through a shunted Josephson junction. The system is both electronically and mathematically simple, where JJ stands as the sole nonlinear element. Our investigation revealed that the proposed system exhibits either no equilibrium or an infinite number of equilibria. The stability analysis of the steady states revealed the system's ability to demonstrate extreme multistability with hidden and self-excited dynamics. The numerical results captured through bifurcation diagrams, spectra of Lyapunov exponents, time series, phase portraits, and basins of initial states, have highlighted some remarkable features. Particularly, the stair-like layers appearing in the three superimposed bifurcation diagrams, captured from parallel branches, reveal the multi-scroll dynamics within the investigated system. This evidence of multi-scrolls is further confirmed through the phase diagrams for discrete values of the main control parameter. In addition, volume expansion of the system was also confirmed through the depicted phase portraits. Among other key findings, our proposed system has exhibited the capability of generating attractors with similar and/or different shapes, also known as homogeneous and heterogeneous multistability, purely by tuning the initial conditions and/or system parameters. Various phase portraits, alongside their corresponding basins of attraction, support these striking phenomena of homogeneous and heterogeneous extreme multistability.

Additionally, the rare phenomenon of tri-transient chaos was captured and discussed within the investigated system. Our results from the time series, associated with the statistical tool of the finite-time Lyapunov exponent, have confirmed the metastable phenomenon in the system. The outcomes of our theoretical and numerical analysis align perfectly with laboratory measurements. Our future investigations will relate on potential industrial applications of the homogeneous and heterogeneous multistability.⁶⁸

AUTHOR DECLARATIONS

Conflict of Interest

The authors have no conflicts to disclose.

Author Contributions

T. Fonzin Fozin: Conceptualization (lead); Formal analysis (lead); Investigation (lead); Methodology (equal); Validation (equal); Visualization (equal); Writing – original draft (equal). A. R. Tchamda: Conceptualization (equal); Formal analysis (lead); Investigation (lead); Methodology (lead); Validation (equal); Visualization (equal); Writing – original draft (equal). G. Sivaganesh: Conceptualization (equal); Formal analysis (lead); Investigation (lead); Methodology (lead); Validation (equal); Writing – original draft (equal). K. Srinivasan: Methodology (equal); Validation (equal); Visualization (equal); Writing – original draft (equal). Z. Tabekoueng Njitacke: Methodology (equal); Validation (equal); Visualization (equal); Writing – original draft (equal). A. B. Mezatio: Investigation (equal); Methodology (equal); Visualization (equal); Writing – original draft (equal).

DATA AVAILABILITY

The data that support the findings of this study are available from the corresponding author upon reasonable request.

REFERENCES

- ¹Z. Wang, C. Volos, S. T. Kingni, A. T. Azar, and V.-T. Pham, Optik 131, 1071 (2017).
- ²D. Chang, Z. Li, M. Wang, and Y. Zeng, AEU Int. J. Electron. Commun. 88, 20 (2018).
- ³R. Ramamoorthy, S. S. Jamal, I. Hussain, M. Mehrabbeik, S. Jafari, and K. Rajagopal, Complexity 2021, 8068737.
- ⁴G. D. Leutcho, L. Woodward, and F. Blanchard, Chaos 33, 103131 (2023).
- ⁵J. C. Sprott, Int. J. Bifurcat. Chaos 21, 2391 (2011).
- ⁶H. Bao, Z. Hua, H. Li, M. Chen, and B. Bao, IEEE Trans. Circuits Syst. I: Regul. Pap. **68**, 4534 (2021).
- ⁷Z. N. Tabekoueng, B. Sriram, K. Rajagopal, A. Karthikeyan, and J. Awrejcewicz, Chaos 33, 063153 (2023).
- ⁸R. Kengne, J. T. Mbe, J. Fotsing, A. B. Mezatio, F. J. Ntsafack Manekeng, and R. Tchitnga, Z. Naturforsch. A 78(9), 801–821 (2023).
- ⁹B. Bao, H. Bao, N. Wang, M. Chen, and Q. Xu, Chaos, Solitons Fractals **94**, 102 (2017)
- ¹⁰B. Ramakrishnan, A. Durdu, K. Rajagopal, and A. Akgul, AEU Int. J. Electron. Commun. 123, 153319 (2020).
- ¹¹T. F. Fozin, B. K. Nzoko, N. A. K. Telem, Z. T. Njitacke, A. A. N. Mouelas, and J. Kengne, Phys. Scr. **97**, 075204 (2022).
- ¹²B. Bao, J. Hu, J. Cai, X. Zhang, and H. Bao, Nonlinear Dyn. 111, 3765 (2023).
- ¹³S. K. Dana, D. C. Sengupta, and K. D. Edoh, IEEE Trans. Circuits Syst. I: Fundam. Theory Appl. 48, 990 (2001).

- ¹⁴I. K. Ngongiah, B. Ramakrishnan, Z. T. Njitacke, G. F. Kuiate, and S. T. Kingni, <u>Phys. A: Stat. Mech. Appl.</u> **603**, 127757 (2022).
- ¹⁵B. D. Josephson, Phys. Lett. **1**, 251 (1962).
- ¹⁶A. Belcher, J. Williams, J. Ireland, R. Iuzzolino, M. E. Bierzychudek, R. Dekker, J. Herick, R. Behr, and K. Schaapman, in *Journal of Physics: Conference Series* (IOP Publishing, 2018), Vol. 1065, p. 052044.
- ¹⁷W. Chen, V. Patel, and J. E. Lukens, Microelectron. Eng. 73, 767 (2004).
- ¹⁸J. T. Fossi, V. Deli, H. C. Edima, Z. T. Njitacke, F. F. Kemwoue, and J. Atangana, Eur. Phys. J. B 95, 66 (2022).
- ¹⁹D. J. Reilly, npj Quantum Inf. 1, 15011 (2015).
- ²⁰ A. I. Braginski, J. Supercond. Novel Magn. **32**, 23 (2019).
- ²¹ A. Leitenstorfer, A. S. Moskalenko, T. Kampfrath, J. Kono, E. Castro-Camus, K. Peng, N. Qureshi, D. Turchinovich, K. Tanaka, A. G. Markelz *et al.*, J. Phys. D: Appl. Phys. **56**, 223001 (2023).
- ²²S. T. Kingni, K. Rajagopal, S. Çiçek, A. Cheukem, V. K. Tamba, and G. F. Kuiate, Eur. Phys. J. B **93**, 44 (2020).
- ²³ P. Louodop, R. Tchitnga, F. F. Fagundes, M. Kountchou, V. K. Tamba, H. A. Cerdeira *et al.*, Phys. Rev. E **99**, 042208 (2019).
- ²⁴F. C. Talla, R. Tchitnga, P. L. Fotso, R. Kengne, B. Nana, and A. Fomethe, Int. J. Bifurcat. Chaos 30, 2050097 (2020).
- $\bf ^{25}$ Y. J. Monkam, S. T. Kingni, R. Tchitnga, and P. Woafo, Analog Integr. Circuits Signal Process. $\bf 110$, 395–407 (2022).
- ²⁶M. E. Yalçin, J. A. Suykens, and J. Vandewalle, IEEE Trans. Circuits Syst. I: Regul. Pap. 51, 1395 (2004).
- ²⁷J. A. Suykens and J. Vandewalle, Cellular Neural Networks, Multi-Scroll Chaos and Synchronization (World Scientific, 2005), Vol. 50.
- ²⁸Q. Wan, F. Li, S. Chen, and Q. Yang, Chaos, Solitons Fractals **169**, 113259 (2023).
- ²⁹ J. M. M. Pacheco and E. T. Cuautle, *Electronic Design Automation of Multi-Scroll Chaos Generators* (Bentham Science Publishers, 2010).
- ³⁰Q. Hong, Q. Xie, Y. Shen, and X. Wang, Chaos **26**, 083110 (2016).
- ³¹ N. Wang, C. Li, H. Bao, M. Chen, and B. Bao, IEEE Trans. Circuits Syst. I: Regul. Pap. **66**, 4767 (2019).
- ³²B. Bao, L. Zhu, X. Wang, Z. Liu, and J. Xu, in 2010 International Conference on Communications, Circuits and Systems (ICCCAS) (IEEE, 2010), pp. 747–751.
- ³³Z. Chen, G. Wen, H. Zhou, and J. Chen, Optik 130, 594 (2017).
- ³⁴Q. Lai, Z. Wan, and P. D. K. Kuate, IEEE Trans. Circuits Syst. I: Regul. Pap. **70**, 1324 (2022).
- 35 J. Lü and G. Chen, Int. J. Bifurcat. Chaos 16, 775 (2006).
- ³⁶J. Ma, X. Wu, R. Chu, and L. Zhang, Nonlinear Dyn. **76**, 1951 (2014).
- 37 M. E. Yalçin, Chaos, Solitons Fractals 34, 1659 (2007).
- ³⁸J. C. Sprott, Int. J. Bifurcat. Chaos 24, 1450009 (2014).
- ³⁹D. Veeman, M. Mehrabbeik, H. Natiq, K. Rajagopal, S. Jafari, and I. Hussain, Int. J. Bifurcat. Chaos **32**, 2230007 (2022).
- ⁴⁰T. F. Fozin, G. Leutcho, A. T. Kouanou, G. Tanekou, R. Kengne, J. Kengne, and F. Pelap, Z. Naturforsch. A 75, 11 (2019).
- ⁴¹G. Sivaganesh, K. Srinivasan, T. F. Fozin, and R. G. Pradeep, Chaos, Solitons Fractals 174, 113884 (2023).

- ⁴²Z. T. Njitacke, B. Ramakrishnan, K. Rajagopal, T. F. Fozin, and J. Awrejcewicz, Chaos. Solitons Fractals 164, 112717 (2022)
- ⁴³Z. T. Njitacke, J. Awrejcewicz, A. N. K. Telem, T. F. Fozin, and J. Kengne, IEEE Trans. Circuits Syst. II: Express Briefs **70**, 791 (2022).
- ⁴⁴G. Vivekanandhan, H. Natiq, A. Ghaffari, A. Bayani, K. Rajagopal, and S. Jafari, Phys. Scr. 98, 115207 (2023).
- ⁴⁵Y. Yang, L. Huang, J. Xiang, and Q. Guo, IEEE Trans. Circuits Syst. II: Express Briefs **69**, 1792 (2021).
- ⁴⁶M. E. Yalçın and J. A. Suykens, in *Proceedings of the 2005 International Symposium on Nonlinear Theory and Its Applications (NOLTA 2005), Bruges, Belgium* (2005), pp. 501–514.
- ⁴⁷S. Takougang Kingni, G. Fautso Kuiate, R. Kengne, R. Tchitnga, and P. Woafo, Complexity 2017, 4107358.
- ⁴⁸B. Ramakrishnan, L. M. A. Tabejieu, I. K. Ngongiah, S. T. Kingni, R. T. Siewe, and K. Rajagopal, J. Supercond. Novel Magn. 34, 2761–2769 (2021).
- ⁴⁹M. Itoh, Int. J. Bifurcat. Chaos **11**, 605 (2001).
- ⁵⁰S. H. Strogatz, Nonlinear Dynamics and Chaos: With Applications to Physics, Biology, Chemistry, and Engineering (Westview Press, 2014).
- ⁵¹ M. Lakshmanan and D. V. Senthilkumar, *Dynamics of Nonlinear Time-Delay Systems* (Springer Science & Business Media, 2011).
- ⁵²V.-T. Pham, C. Volos, S. Jafari, and T. Kapitaniak, Nonlinear Dyn. **87**, 2001 (2017).
- ⁵³B. Bao, J. Luo, H. Bao, C. Chen, H. Wu, and Q. Xu, Int. J. Bifurcat. Chaos **29**, 1950168 (2019).
- ⁵⁴ A. Wolf, J. B. Swift, H. L. Swinney, and J. A. Vastano, Phys. D: Nonlinear Phenom. **16**, 285 (1985).
- ⁵⁵G. D. Leutcho, J. Kengne, T. Fonzin Fozin, K. Srinivasan, Z. Njitacke Tabekoueng, S. Jafari, and M. Borda, J. Comput. Nonlinear Dyn. 15, 051004 (2020).
- ⁵⁶C. Li and J. C. Sprott, Optik **127**, 10389 (2016).
- ⁵⁷C. Li, T. Lei, X. Wang, and G. Chen, Chaos **30**, 063124 (2020).
- ⁵⁸S. Zhang, J. Zheng, X. Wang, Z. Zeng, and S. He, Nonlinear Dyn. **102**, 2821 (2020)
- ⁵⁹ X. Zhou, C. Li, Y. Li, X. Lu, and T. Lei, Nonlinear Dyn. **105**, 1843 (2021).
- ⁶⁰I. Obeid, J. C. Morizio, K. A. Moxon, M. A. Nicolelis, and P. D. Wolf, IEEE Trans. Biomed. Eng. **50**, 255 (2003).
- ⁶¹S. Sabarathinam and K. Thamilmaran, Nonlinear Dyn. **87**, 2345 (2017).
- ⁶² A. Chithra, T. F. Fozin, K. Srinivasan, E. R. M. Kengne, A. T. Kouanou, and I. R. Mohamed, Int. J. Bifurcat. Chaos 31, 2150049 (2021).
- 63 S. Yan, E. Wang, and Q. Wang, Chaos 33, 033107 (2023).
- 64H. Wu and X. Wang, IEEE Trans. Ind. Electron. 66, 6473 (2018).
- ⁶⁵S. Yan, E. Wang, B. Gu, Q. Wang, Y. Ren, and J. Wang, Phys. A: Stat. Mech. Appl. **602**, 127652 (2022).
- ⁶⁶G. Sivaganesh, K. Srinivasan, T. Fonzin Fozin, and R. Gladwin Pradeep, Chaos 33, 093116 (2023).
- 67 S. Sabarathinam and K. Thamilmaran, Chaos, Solitons Fractals 73, 129 (2015)
- ⁶⁸E. Fadil, A. Abass, and S. Tahhan, Opt. Quantum Electron. 54, 477 (2022).